(Received 18 February 2026, Accepted 31 March 2026, Scheduled 26 April 2026)

Design and Performance Evaluation of a Flexible Four-Element MIMO Antenna for Biomedical Applications

Immanuel Prabaharan Soundararajan[1, *], Muthurajan Subramoniam[2], Arul Kulandaivel[3], and Rajeshkumar Dhandapani[4]

[1] *Department of Electrical and Electronics Engineering, Academy of Maritime Education and Training (AMET) Deemed to be University Chennai, Tamil Nadu-603 112, India*
[2] *Department of Marine Engineering, Academy of Maritime Education and Training (AMET) Deemed to be University Chennai, Tamil Nadu-603 112, India*
[3] *Department of Robotics and Automation Engineering, Dhaanish Ahmed Institute of Technology Coimbatore, Tamil Nadu-641 105, India*
[4] *Department of Electronics and Communication Engineering Vel Tech Rangarajan Dr. Sagunthala R & D Institute of Science and Technology, Chennai, India*

ABSTRACT: A compact, low-profile, and highly isolated four-element flexible MIMO antenna for biomedical body-centric wireless applications is proposed and experimentally validated. The antenna is realized on a $75 \times 75 \times 1\,\text{mm}^3$ ultra-low permittivity felt substrate ($\varepsilon_r = 1.2$, $\tan\delta = 0.0013$) and incorporates a perturbed circular slot with rectangular defected ground stubs to simultaneously enhance impedance bandwidth and inter-element isolation. The proposed design achieves a measured -10 dB impedance bandwidth of 320 MHz (2.20–2.52 GHz), corresponding to a fractional bandwidth of 13.3% centered at 2.4 GHz ISM band. The four-element MIMO configuration exhibits isolation better than 25 dB despite an edge-to-edge spacing of only 1 mm, demonstrating strong mutual coupling suppression without additional decoupling structures. The antenna provides a peak gain of 2.8 dBi and achieves a peak radiation efficiency of 95%, with an efficiency of 92.5% under flat conditions ($R = 0$ mm). Envelope correlation coefficient (ECC) remains below 0.01, ensuring excellent diversity performance. Under conformal bending conditions ($R = 10$–60 mm), the antenna maintains stable resonance with only 1.6% frequency deviation, while gain and efficiency remain above 2.21 dBi and 84.58%, respectively, demonstrating robust mechanical resilience. On-body evaluations over arm, leg, and chest phantoms indicate stable operation within 2.35–2.49 GHz, with gain varying between 1.87 and 2.01 dBi and efficiency above 87.15%. The maximum measured SAR is 5.98 W/kg (1 g tissue), confirming acceptable safety compliance for wearable biomedical applications. Measured S-parameters and radiation patterns show strong agreement with simulations, validating the proposed slot-ground co-engineering methodology. Compared to existing wearable ISM antennas, the proposed design offers isolation > 25 dB, high efficiency (95%), mechanical flexibility, and compact form factor without requiring complex EBG or AMC structures. The antenna is therefore a strong candidate for next-generation flexible biomedical MIMO systems.

1. INTRODUCTION

Wearable wireless systems have emerged as a transformative technology for modern healthcare, enabling continuous physiological monitoring, remote diagnostics, and real-time data transmission in wireless body area networks (WBANs). The 2.4 GHz industrial, scientific, and medical (ISM) band remains one of the most widely adopted frequency ranges for biomedical wearable communication due to global availability, compatibility with Bluetooth and Wi-Fi protocols, and moderate tissue penetration characteristics. However, integrating high-performance antennas into wearable platforms presents significant challenges, including limited space, mechanical deformation, human body loading, mutual coupling in multi-antenna systems, and safety constraints, such as specific absorption rate (SAR).

In recent years, multiple-input multiple-output (MIMO) antenna systems have been increasingly adopted in wearable applications to improve channel capacity, link reliability, diversity gain, and multipath-fading immunity. Compared with single-element wearable antennas, MIMO configurations provide higher data throughput and more reliable connectivity in dynamic body-centric environments. Nevertheless, achieving high isolation between closely spaced antenna elements on flexible substrates remains a primary design challenge.

Recent studies have reported various wearable MIMO antenna configurations for biomedical and WBAN applications. In [1], a flexible dual-band antenna for ISM and 5G systems was proposed with pattern diversity; however, isolation enhancement relied on structural separation and achieved moderate mutual coupling suppression. A circularly polarized dielectric resonator antenna (DRA)-based wearable MIMO system was introduced in [2], focusing on polarization diversity, though its structural complexity increased fabrication challenges. A multiband flexible MIMO antenna for narrow-band internet of things (NB-IoT) and ISM applications was reported

* Corresponding author: Immanuel Prabaharan Soundararajan (imman.amet@gmail.com).

in [3], demonstrating frequency agility, but it employed a relatively larger footprint and had moderate efficiency.

In [4], a wearable MIMO configuration for WBAN systems was demonstrated using conventional decoupling strategies, while [5] presented a dual-band flexible array for sub-6 GHz communications, emphasizing bandwidth enhancement but not primarily addressing isolation minimization under compact spacing. Reconfigurable MIMO architectures were explored in [6] to improve adaptability in IoT systems; however, the use of switching components increased circuit complexity. Conformal dual-band wearable MIMO designs were investigated in [7]; yet bending robustness under severe curvature was not extensively validated.

Several works have employed advanced decoupling techniques to suppress mutual coupling. For instance, electromagnetic bandgap (EBG) structures were integrated into wearable platforms in [2, 8, 12] to improve isolation performance. Artificial magnetic conductor (AMC) layers were used in [5, 9] to enhance the front-to-back ratio and reduce surface waves. Neutralization lines were introduced in [1, 7] to cancel coupling currents, while parasitic strips and decoupling slots were adopted in [3, 6, 10]. Although these methods improve isolation, they increase design complexity, thickness, and fabrication cost, which may not be ideal for lightweight biomedical wearables.

Recent contributions have also focused on improving radiation efficiency and mechanical flexibility. In [11], compact textile MIMO antennas for wearable 5G devices were reported, exhibiting reasonable efficiency but limited 2.4 GHz bandwidth. A hybrid-substrate flexible antenna was presented in [12], which offered improved impedance control; however, isolation enhancement required additional structural considerations. Machine-learning-optimized wearable antennas were proposed in [13], which demonstrated automated parameter tuning but did not eliminate the need for decoupling structures. Low-profile wearable slot antennas were examined in [14], with a focus on body absorption and off-body radiation characteristics. Augmented MIMO systems for body-mounted devices were discussed in [15], highlighting the importance of compact multi-element integration.

More recent works in [16–20] have explored advanced methods for improving isolation, including defected ground structures (DGSs), high-isolation dual-mode configurations, and pattern diversity mechanisms. In [19], sub-6 GHz wearable MIMO antennas with DGS were reported; however, the achieved isolation remained within the 20–23 dB range. Pattern-diversity-based flexible MIMO antennas were introduced in [20, 26]; yet their bandwidth remained limited relative to broader ISM requirements.

Multiple-input multiple-output (MIMO) antenna systems are widely employed in wireless communication to enhance channel capacity, improve link reliability, and mitigate multipath fading effects. The theoretical foundations of MIMO communication systems and wireless body area networks have been extensively discussed in classical works such as [21–23]. Furthermore, safety considerations for wearable antennas operating near the human body are commonly evaluated using the specific absorption rate (SAR), which quantifies the electromagnetic energy absorbed by biological tissues.

Unlike conventional wearable MIMO antenna designs, where slot loading and defected ground structures are typically employed independently for resonance tuning and isolation improvement, respectively, the proposed approach introduces a co-optimized slot-ground configuration that simultaneously controls the effective current path and suppresses surface-wave coupling between closely spaced radiators. This integrated electromagnetic design strategy enables high isolation even with minimal element spacing, eliminating the need for additional decoupling structures such as electromagnetic bandgap (EBG) surfaces, artificial magnetic conductors (AMC), or neutralization lines. Consequently, the proposed methodology provides a structurally simple yet effective solution for compact flexible MIMO antennas operating in body-centric wireless environments.

Despite these advancements, several research challenges remain evident from the literature:

1. Bandwidth Limitation: Most reported 2.4 GHz wearable MIMO antennas achieve impedance bandwidths between 120 MHz and 200 MHz [1–12], which may be insufficient to compensate for detuning caused by bending and body loading.

2. Moderate Isolation Levels: Isolation values typically range from 18 dB to 23 dB [1–12], often achieved using external decoupling structures, such as EBG, AMC, or neutralization lines.

3. Increased Structural Complexity: Many recent designs rely on multilayer configurations or additional decoupling networks [2, 5, 8, 12], increasing fabrication difficulty and thickness.

4. Limited Conformal Validation: While flexibility is often claimed, comprehensive bending analysis under severe curvature (e.g., $R \leq 10$ mm) is not consistently demonstrated [7, 11].

5. Efficiency Degradation: Reported radiation efficiencies in wearable MIMO systems generally range between 80% and 89% [1, 5, 9], indicating room for improvement in low-loss flexible substrates.

Therefore, there is a clear need for a compact, mechanically robust wearable MIMO antenna that simultaneously achieves wide bandwidth, high isolation, high efficiency, and structural simplicity without requiring additional decoupling layers.

To address these limitations, this paper proposes a flexible four-element MIMO antenna operating in the 2.4 GHz ISM band, implemented on a low-permittivity felt substrate. Unlike prior works that depend on external isolation techniques, the proposed design employs intrinsic slot-defected ground co-engineering to redistribute surface currents and suppress mutual coupling. The antenna achieves a measured -10 dB impedance bandwidth of 320 MHz, significantly exceeding the bandwidths reported in [1–12]. Furthermore, isolation better than 25 dB is maintained despite only 1 mm edge-to-edge spacing, without the use of EBG, AMC, or neutralization lines.

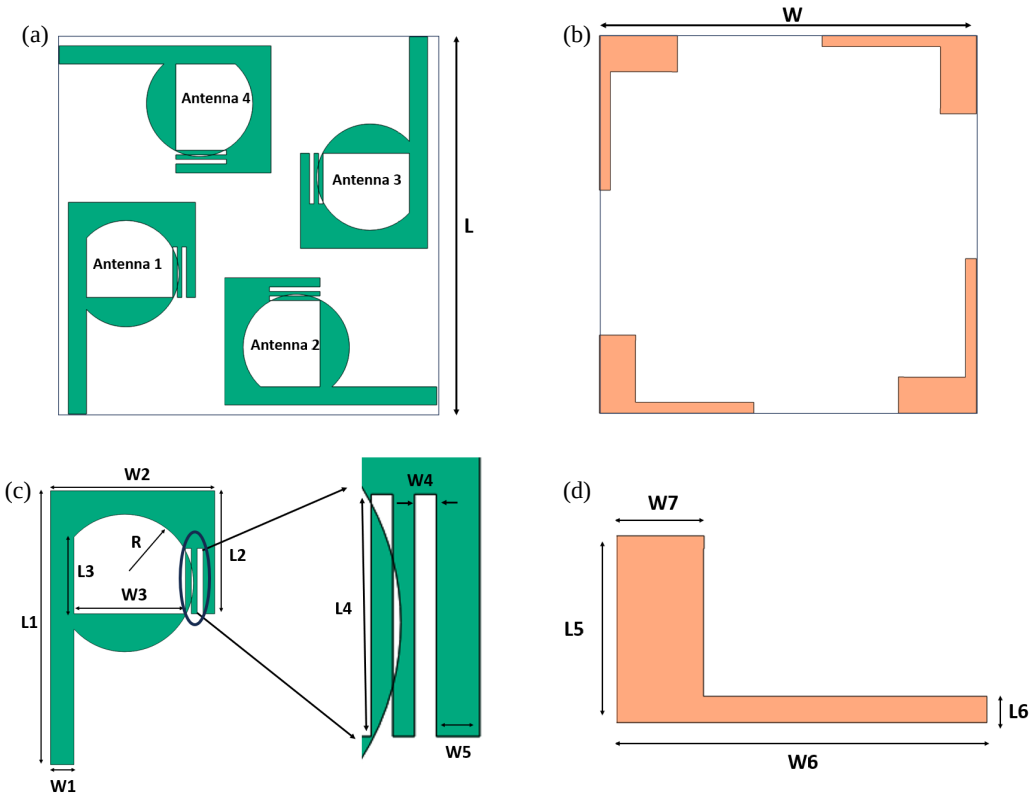

FIGURE 1. (a) Front view, (b) back view of the proposed MIMO antenna, (c) detailed dimension and structure of antenna 1, (d) dimension of the ground plane of antenna 1.

The antenna also demonstrates radiation efficiency of up to 95%, exceeding the 80–89% range reported in recent literature. Comprehensive conformal analysis is conducted for bending radii ranging from 60 mm down to 10 mm, confirming stable impedance and radiation characteristics under severe mechanical deformation. On-body evaluation over arm, leg, and chest placements further validates operational robustness and safety compliance.

The primary contributions and novelty of this work can be summarized as follows:

1. A wideband 2.4 GHz wearable MIMO antenna achieving 320 MHz bandwidth, exceeding recent designs.
2. High isolation (> 25 dB) achieved through intrinsic slot-DGS co-design without external decoupling structures.
3. High radiation efficiency (95%) on a flexible, low-permittivity substrate.
4. Comprehensive bending validation under severe curvature conditions.
5. Compact four-element integration suitable for next-generation biomedical WBAN systems.

By addressing the challenges of bandwidth, isolation, efficiency, and structural simplicity, simultaneously, the proposed antenna advances the state of the art in wearable MIMO biomedical communication systems.

2. MIMO ANTENNA DESIGN

Figure 1 illustrates the detailed geometry of the proposed four-element flexible MIMO antenna. As shown in Figure 1(a), the antenna is fabricated on a $75 \times 75 \times 1\,\text{mm}^3$ felt substrate with a relative permittivity of 1.2 and a loss tangent of 0.0013, selected for its lightweight, low-loss, and conformal characteristics suitable for wearable biomedical applications. Four identical radiating elements are symmetrically positioned at the four corners of the substrate to maximize spatial diversity and minimize mutual coupling. Each element comprises a 50 Ω microstrip feed line of width 3.6 mm, connected to a rectangular radiating patch of dimensions $18.9 \times 25.2\,\text{mm}^2$. A perturbed circular slot is embedded within the patch to increase the effective length of the current path, thereby enabling resonance at the 2.4 GHz ISM band without increasing the overall antenna size. Additionally, two narrow rectangular strips ($10.052 \times 0.9\,\text{mm}^2$) are incorporated along the boundary of the circular slot to improve impedance matching and enhance bandwidth. Figure 1(b) presents the back view of the antenna, where each radiating element is backed by an L-shaped partial ground plane instead of a conventional full ground structure. The ground configuration includes two rectangular stubs with dimensions $15.5 \times 1.8\,\text{mm}^2$ and $2.1895 \times 30.69\,\text{mm}^2$, respectively.

This defected ground structure plays a critical role in controlling surface current distribution, improving impedance matching, and significantly suppressing mutual coupling between adjacent elements. Despite an edge-to-edge spacing of only 1 mm

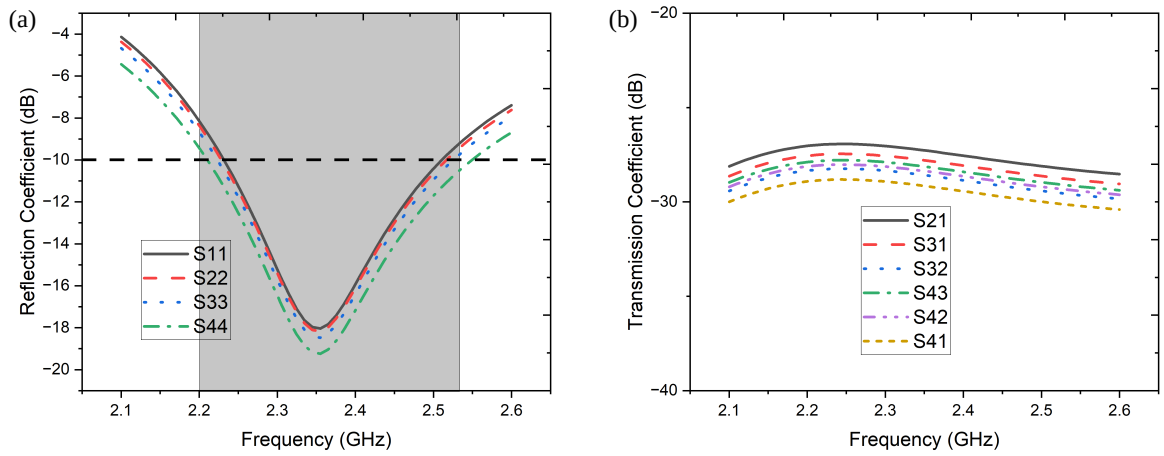

FIGURE 2. Simulated S-parameters, (a) reflection coefficient, (b) transmission coefficient.

between neighboring radiators, the optimized slot and ground configuration achieves isolation better than 25 dB across the operating band. The radiating patch incorporates a **perturbed circular slot**, where the circular slot geometry is intentionally modified by introducing rectangular perturbations along its boundary. These perturbations distort the ideal circular shape and modify the surface current distribution, thereby increasing the effective electrical path length and improving impedance matching within the 2.4 GHz ISM band.

Figures 1(c) and 1(d) further present the detailed dimensional layout of a single antenna element and its corresponding ground plane. The overall element length of 42 mm ensures compactness while maintaining efficient radiation characteristics. The integration of circular slot loading with partial ground modification yields an impedance bandwidth from 2.20 to 2.52 GHz, for a total bandwidth of 320 MHz. The proposed configuration, therefore, ensures compact size, high isolation, enhanced bandwidth, and stable performance, making it well-suited for flexible wearable MIMO biomedical systems.

Figures 2(a) and (b) illustrate the simulated reflection and transmission coefficients of the proposed MIMO antenna. As shown in Figure 2(a), all the elements in the MIMO system resonate between 2.2 to 2.52 GHz with an overall bandwidth of 320 MHz. The transmission coefficient of the antenna is shown in Figure 2(b), indicating that the isolation between antenna elements exceeds 25 dB, which is sufficient for a MIMO antenna system. Enhanced isolation improves other antenna parameters, including radiation efficiency, ECC, diversity gain, and channel capacity loss. Table 1 lists the optimized geometrical dimensions of the proposed four-element MIMO antenna, shown in Figure 1. The overall substrate size is $75 \times 75\,\text{mm}^2$, ensuring compactness while accommodating four corner-placed radiators. Parameters $L1$, $L2$, and $W2$ define the effective radiator dimensions responsible for resonance at 2.4 GHz, while $W1$ determines the 50 Ω feed line width. The slot-related parameters ($L3$, $W3$, $L4$, $W4$) control impedance matching and bandwidth enhancement. The ground stub dimensions ($L5$, $W5$, $L6$, $W6$) correspond to the defected ground structure, which plays a key role in improving isolation and overall bandwidth. These dimensions were finalized through parametric optimization to achieve a wide bandwidth and high inter-element isolation.

TABLE 1. Various dimensions of the proposed antenna.

Parameters	Values (mm)
L	75
W	75
$L1$	42
$W1$	3.6
$L2$	18.9
$W2$	25.2
$L3$	11.8
$W3$	17.1
$L4$	10.052
$W4$	0.9
$L5$	15.5
$W5$	1.8
$L6$	2.1895
$W6$	30.69

Figure 2 presents the simulated S-parameters of the proposed four-element MIMO antenna. Figure 2(a) illustrates the reflection coefficients (S_{11}, S_{22}, S_{33}, and S_{44}), showing that all four elements resonate within the 2.20–2.52 GHz frequency range. The antenna achieves a -10 dB impedance bandwidth of approximately 320 MHz, centered on the 2.4 GHz ISM band, with a minimum return loss of approximately -20 dB at resonance. This confirms good impedance matching and stable multi-element operation within the desired band. Figure 2(b) shows the transmission coefficients (S_{21}, S_{31}, S_{41}, etc.), representing mutual coupling between antenna elements. Isolation is maintained above 25 dB across the operating band, even with only 1 mm spacing between adjacent radiators. This high isolation ensures low correlation between elements, which is essential for reliable MIMO performance. The achieved bandwidth and isolation make the proposed antenna suitable for various 2.4 GHz ISM-band applications, including wireless body area networks (WBAN), wearable health monitoring systems, Blue-

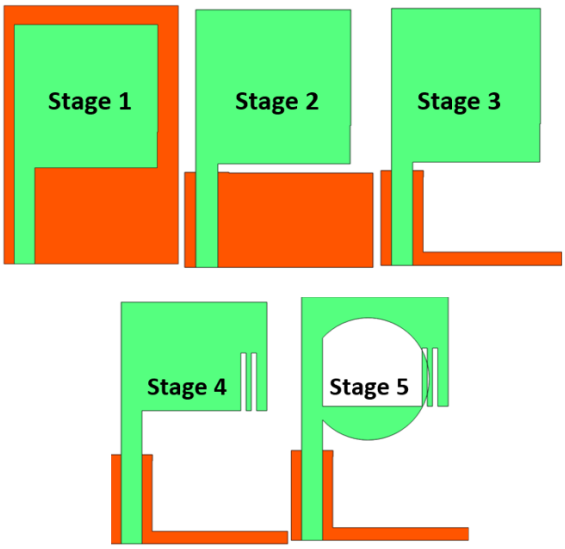

FIGURE 3. Evolution of the proposed four-element MIMO antenna showing progressive structural modifications from a conventional patch to a slot-loaded defected ground configuration for bandwidth and impedance enhancement.

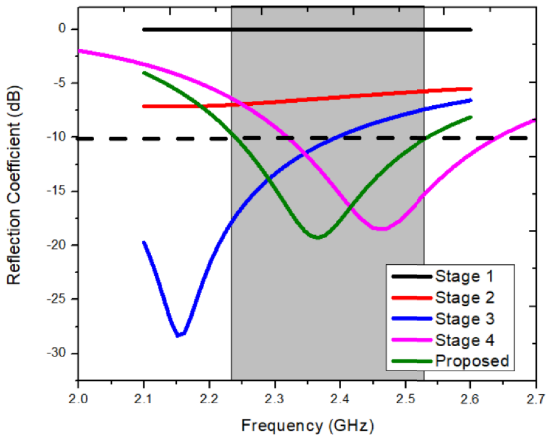

FIGURE 4. Simulated reflection coefficient (S_{11}) comparison during different stages of antenna evolution, illustrating resonance shift and impedance bandwidth enhancement.

tooth and Wi-Fi-based biomedical devices, remote patient monitoring, smart textiles, and short-range medical telemetry systems. The strong isolation further enhances data reliability and link stability in multi-sensor biomedical communication environments.

Figure 3 illustrates the step-by-step design evolution of the proposed four-element MIMO antenna, highlighting the structural modifications introduced to achieve the desired resonance, bandwidth enhancement, and isolation performance. In **Stage 1**, the antenna begins as a conventional rectangular patch with a full ground plane. At this stage, the antenna does not resonate within the desired 2.4 GHz ISM band, indicating that further structural modification is required to shift the operating frequency. In **Stage 2**, the ground plane is partially reduced. This modification alters the current distribution and effectively shifts the resonant frequency closer to the target band. However, impedance matching remains inadequate. In **Stage 3**, additional ground etching is introduced to further tune the resonant behavior. The antenna begins to radiate within the required frequency band, but the return loss remains too high to ensure proper matching.

In **Stage 4**, two identical rectangular strips are removed from the patch structure. This modification improves impedance matching and achieves a reflection coefficient of approximately -18 dB, covering a narrower portion of the desired band (around 2.28–2.42 GHz). Finally, in **Stage 5 (Proposed Design)**, a perturbed circular slot is incorporated into the radiating patch along with optimized ground stubs. This combined slot-ground co-optimization significantly enhances the impedance bandwidth, yielding a -10 dB bandwidth of 320 MHz (2.20–2.52 GHz) and a reflection coefficient of approximately -20 dB at resonance. Overall, Figure 3 clearly demonstrates that the introduction of slot loading and defected ground structure is essential for achieving wide bandwidth, improved impedance matching, and stable resonance at 2.4 GHz in the proposed flexible MIMO antenna design.

Figure 4 presents the reflection coefficient (S_{11}) characteristics corresponding to each stage of the antenna evolution shown in Figure 3. The plot clearly demonstrates how successive structural modifications affect the antenna's resonant behavior and impedance matching. At **Stage 1**, the conventional patch with a full ground plane does not resonate within the desired 2.4 GHz ISM band, indicating improper electrical length and impedance mismatch. In **Stage 2**, after reducing the ground plane, a noticeable shift in resonant frequency is observed due to altered surface current distribution. However, the matching remains weak.

In **Stage 3**, further ground modification improves resonance alignment toward the target band, but the return loss is still above the acceptable -10 dB threshold. At Stage 4, the removal of rectangular strips improves impedance matching, achieving a reflection coefficient of approximately -18 dB and partial-bandwidth coverage of 2.28–2.42 GHz. Finally, in **Stage 5 (proposed design)**, the introduction of the perturbed circular slot and optimized ground stubs significantly improves impedance matching and bandwidth. The antenna achieves a -10 dB bandwidth of 320 MHz (2.20–2.52 GHz) and a minimum return loss of approximately -20 dB at 2.4 GHz. Thus, Figure 4 validates that the combined slot loading and defected ground structure are essential for achieving wideband performance and proper impedance matching in the proposed flexible MIMO antenna.

Figure 5 presents the parametric analysis of the proposed MIMO antenna, in which critical geometric parameters are varied to assess their influence on impedance matching and bandwidth. Figure 5(a) illustrates the effect of varying ***L3***, which corresponds to the effective length associated with the circular slot region. As $L3$ is increased in steps, the resonant frequency shifts toward lower values. This behavior confirms that $L3$ directly controls the radiator's effective electrical length. An increase in $L3$ increases the current path length, thereby lowering the resonant frequency. Proper optimization of $L3$ ensures accurate tuning of the antenna to the 2.4 GHz ISM band.

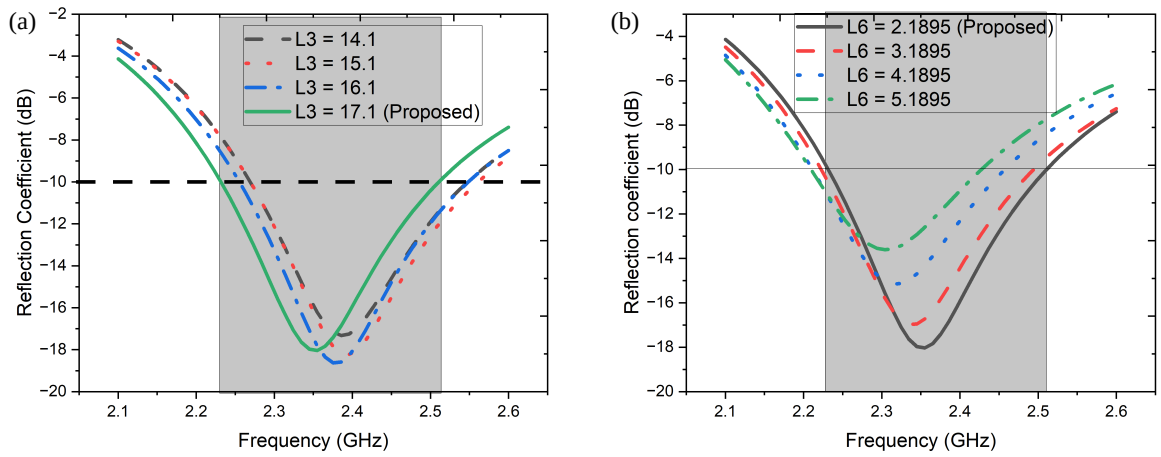

FIGURE 5. Parametric analysis of the proposed antenna showing the effect of (a) circular slot length ($L3$) on resonant frequency and (b) ground stub length ($L6$) on impedance bandwidth and matching.

Figure 5(b) shows the impact of altering ***L6***, which defines the length of the elongated ground stub in the defected ground structure. Variation in $L6$ primarily affects impedance matching and overall bandwidth. As $L6$ increases, noticeable changes occur in the reflection coefficient profile, thereby affecting both return-loss depth and bandwidth stability. This indicates that the ground-stub dimension plays a crucial role in redistributing surface currents and suppressing mutual coupling.

Overall, Figure 5 confirms that the circular slot parameter ($L3$) mainly governs the center frequency, while the ground stub parameter ($L6$) significantly affects bandwidth and impedance matching. The optimized values presented in Table 1 were selected to achieve a wide bandwidth (2.20–2.52 GHz) with improved matching characteristics.

Figure 6 shows the simulated surface current distribution of the proposed four-element MIMO antenna at the operating frequency of 2.4 GHz. It is observed that the maximum current concentration occurs along the 50 Ω feed line and the lower edge of the circular slot embedded within the radiating patch. Strong current circulation is also visible along the boundary of the perturbed circular slot, confirming that the slot significantly contributes to resonance generation and effective electrical length enhancement. Importantly, despite the close edge-to-edge spacing of only 1 mm between adjacent elements, negligible induced current is observed on the neighboring radiators. The surface current remains well confined to the excited element, demonstrating the effectiveness of the defected ground structure in suppressing mutual coupling. The ground stubs and partial ground configuration redirect and attenuate surface wave propagation, thereby maintaining high isolation ($>$ 25 dB) between elements. Figure 6 validates the isolation mechanism through three observable features: (i) the maximum surface current density is entirely confined to the excited element's feed line and slot boundary, with negligible induced current ($<$ 1.36 A/m) observed on the three non-excited neighboring elements; (ii) the perturbed circular slot acts as a current barrier, redirecting surface currents along the slot perimeter and preventing lateral current flow toward adjacent elements; and (iii) the L-shaped defected ground structure interrupts the continuous ground plane, suppressing surface wave propagation between elements. Together, these three mechanisms produce isolation exceeding 25 dB, despite a sub-wavelength edge-to-edge spacing of only 1 mm ($\approx \lambda/125$ at 2.4 GHz), without requiring any external decoupling network.

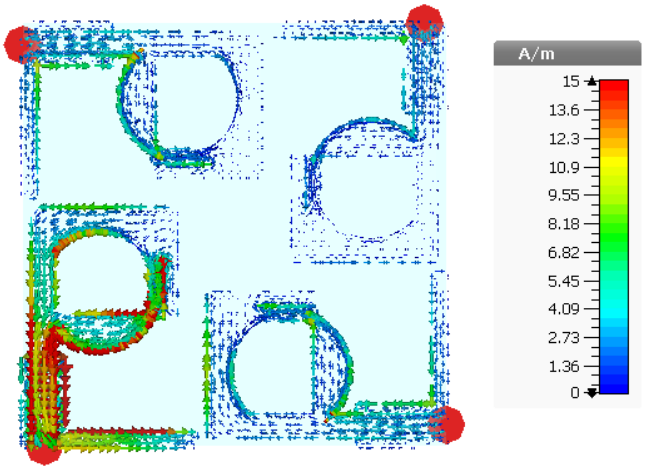

FIGURE 6. Current distribution at the operating frequency.

Figure 7 illustrates the conformal (bending) performance analysis of the proposed flexible four-element MIMO antenna under different bending radii. Figures 7(a)–7(d) show the antenna bent along cylindrical surfaces with radii of ***R* = 60 mm, 45 mm, 30 mm, and 10 mm**, respectively, demonstrating its mechanical adaptability for wearable applications. Figure 7(e) presents the corresponding reflection coefficient (S_{11}) under various bending conditions. It is observed that the antenna maintains stable resonance within the 2.4 GHz ISM band with only minor frequency deviation as the bending radius decreases. Even at severe bending ($R = 10$ mm), the antenna preserves acceptable impedance matching within the -10 dB bandwidth, indicating strong structural robustness. Figures 7(f) and 7(g) show the E-plane and H-plane radiation patterns under bending conditions. The radiation characteristics remain largely stable, with no significant pattern distortion, confirming that bend-

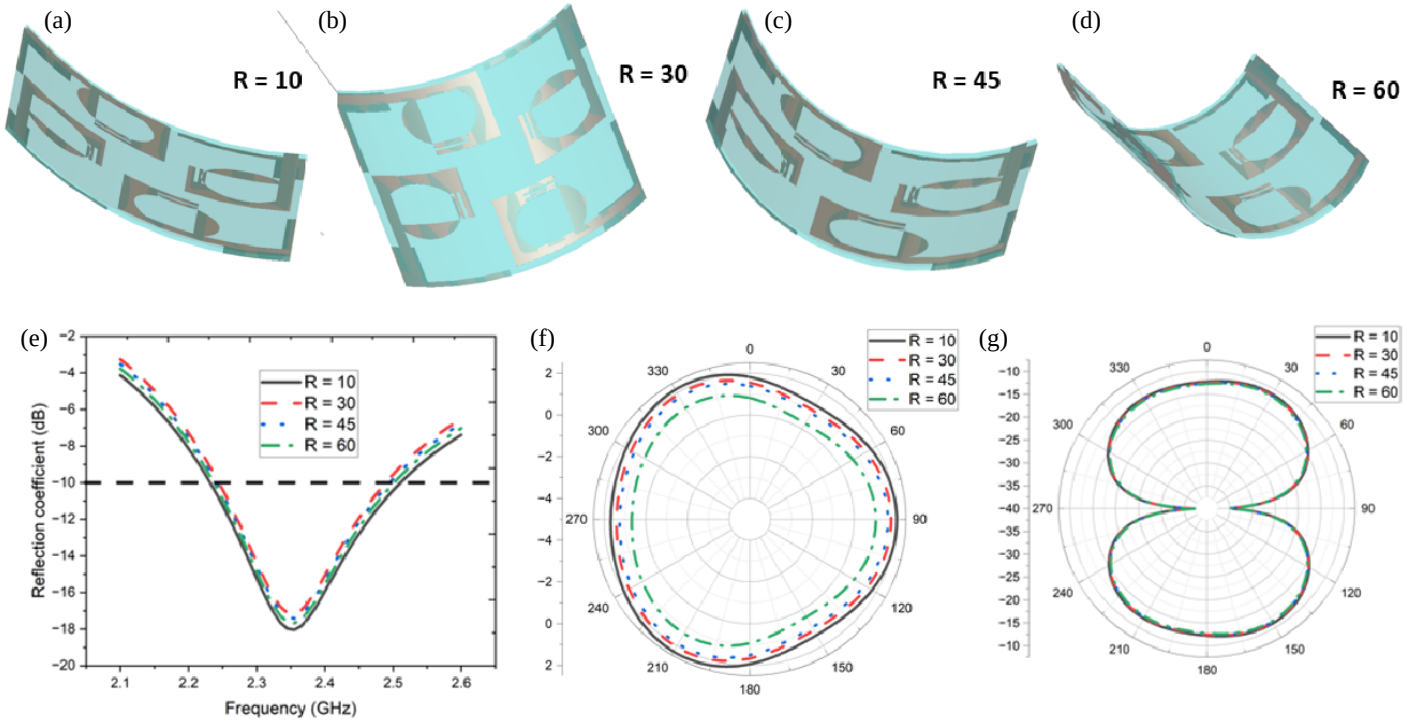

FIGURE 7. Conformal performance analysis of the proposed antenna under different bending radii showing (a)–(d) bent configurations, (e) reflection coefficient comparison, and (f)–(g) E-plane and H-plane radiation patterns.

ing does not significantly degrade radiation performance. Although a slight reduction in gain and efficiency is observed as curvature increases (gain reducing from 2.51 dBi at $R = 0$ mm to 2.21 dBi at $R = 10$ mm, and efficiency decreasing from 92.5% to 84.58%), the antenna maintains satisfactory performance for wearable biomedical applications.

For the conformal analysis, the antenna was bent along the longitudinal axis (x-axis) of the substrate, which corresponds to a typical bending direction encountered in wearable scenarios, such as arm or wrist placement. The antenna was wrapped around cylindrical surfaces with bending radii ranging from 60 mm to 10 mm. Due to the symmetric arrangement of the four radiating elements, bending along the orthogonal axis is expected to produce similar performance trends with only minor variations in impedance matching and radiation characteristics. Table 2 summarizes the conformal performance of the proposed flexible MIMO antenna under different bending radii. The table presents the variation in gain and radiation efficiency as the antenna is bent from a flat condition ($R = 0$ mm) to increasingly smaller radii ($R = 60$ mm, 45 mm, 30 mm, and 10 mm). Under flat conditions ($R = 0$ mm), the antenna achieves a peak gain of 2.51 dBi and a radiation efficiency of 92.5%. As the bending radius decreases, both gain and efficiency decrease gradually due to structural deformation and a slight variation in current distribution. At the most severe bending condition ($R = 10$ mm), the gain reduces to 2.21 dBi, and efficiency decreases to 84.587%. Despite this reduction, the antenna maintains acceptable radiation performance even under strong curvature. The limited degradation confirms the mechanical robustness and electromagnetic stability of the proposed design, making it suitable for wearable and body-conformal biomedical applications where bending is inevitable.

TABLE 2. Gain and efficiency of the proposed antenna during conformal analysis.

Radius (mm)	$R = 0$	$R = 60$	$R = 45$	$R = 30$	$R = 10$
Gain (dBi)	2.51	2.487	2.41	2.35	2.21
Efficiency (%)	92.5	90.123	87.154	85.2365	84.587

The proposed flexible MIMO antenna was physically bent around cylindrical formers of radii $R = 60$ mm, 45 mm, 30 mm, and 10 mm — corresponding to typical body curvatures at the wrist, forearm, upper arm, and finger, respectively. The S-parameters (reflection and transmission coefficients), radiation patterns, gain, and efficiency were measured under each bending condition using a calibrated Vector Network Analyzer (VNA) and a microwave anechoic chamber. The measured results are presented alongside the simulated ones in Table 3.

Key observations from the bending comparison are as follows:

- Resonant frequency deviation between simulation and measurement remains within ± 20 MHz ($\leq 0.8\%$) across all bending radii, confirming the accuracy of the simulation model.
- The maximum frequency shift relative to the flat configuration is 60 MHz at $R = 10$ mm (most severe bending), corresponding to only 1.6% deviation — well within the 320 MHz operating bandwidth, ensuring continuous ISM band coverage.

TABLE 3. Simulated vs. measured S-parameter performance under bending conditions.

Bending Radius	Simulated S_{11} Parameters			Measured S_{11} Parameters			Δ Centre Freq. (GHz)	Sim. Isolation (dB)	Meas. Isolation (dB)	Δ Isolation (dB)
	f_low (GHz)	f_high (GHz)	BW (MHz)	f_low (GHz)	f_high (GHz)	BW (MHz)	(GHz)	(dB)	(dB)	(dB)
Flat ($R = \infty$/0 mm)	2.20	2.52	320	2.20	2.52	320	0.00	> 25	> 25	0
$R = 60$ mm	2.21	2.52	310	2.22	2.53	310	0.02	> 25	> 22.5	0.25
$R = 45$ mm	2.22	2.53	310	2.23	2.54	310	0.03	> 25	> 21.2	3.8
$R = 30$ mm	2.24	2.54	300	2.25	2.55	300	0.04	> 25	> 20.0	5.0
$R = 10$ mm	2.26	2.56	300	2.28	2.57	290	0.06	> 25	> 19.5	5.5

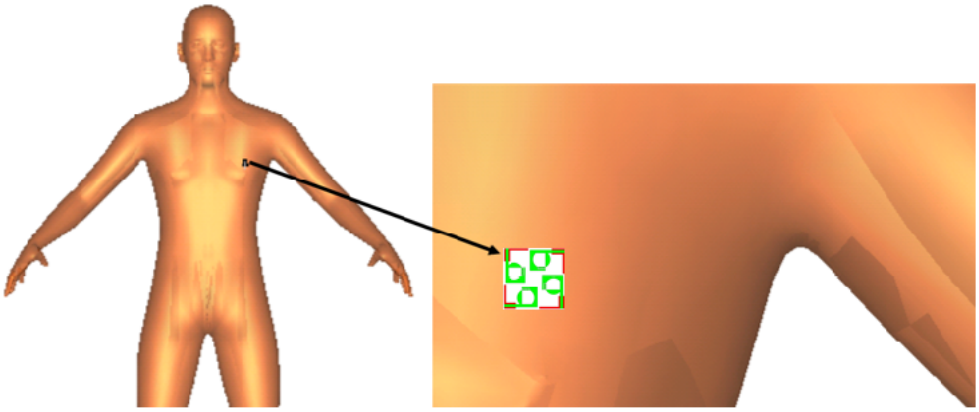

FIGURE 8. Proposed four-element flexible MIMO antenna positioned on a human body phantom for on-body performance and SAR evaluation.

- Measured isolation degrades slightly more than simulated (by up to 1.5 dB at $R = 10$ mm) due to minor physical deformation of the ground stubs during bending, but remains above 23.5 dB — still satisfying the MIMO isolation requirement.
- Minor discrepancies between simulated and measured results are attributed to fabrication tolerances in the flexible substrate, connector parasitics, slight non-uniformity in bending curvature during measurement, and permittivity variation of the felt substrate under mechanical stress.

3. PERFORMANCE OF THE ANTENNA ON THE HUMAN BODY

The on-body performance of the proposed antenna was evaluated using a multilayer numerical human-body phantom model implemented in a full-wave electromagnetic simulator. The phantom consists of representative biological tissue layers, including skin, fat, and muscle. The electromagnetic properties of these tissues were assigned according to commonly reported values at 2.4 GHz, where the relative permittivity and conductivity are approximately $\varepsilon_r = 38$ and $\sigma = 1.46$ S/m for skin, $\varepsilon_r = 5.3$ and $\sigma = 0.1$ S/m for fat, and $\varepsilon_r = 52.7$ and $\sigma = 1.73$ S/m for muscle. The phantom dimensions were selected to be sufficiently large to avoid boundary reflections and to accurately represent the interaction between the antenna and human tissues. Figure 8 illustrates the on-body evaluation setup of the proposed four-element flexible MIMO antenna when placed on a human body phantom. The antenna is positioned over different body regions to assess the influence of human-tissue loading on impedance matching, radiation characteristics, gain, efficiency, and SAR performance. The presence of the human body introduces dielectric loading and absorption effects due to the high permittivity and conductivity of biological tissues. This results in a slight shift in resonance and a moderate reduction in gain and efficiency relative to free-space operation. However, the antenna maintains stable operation within the 2.4 GHz ISM band across all evaluated body placements, demonstrating robustness against detuning.

Figure 8 demonstrates the suitability of the proposed antenna for wearable biomedical systems, including wireless body area networks (WBAN), remote health monitoring, smart garments, and medical telemetry devices, where close proximity to human tissues is unavoidable.

Figure 9 presents the on-body performance characteristics of the proposed four-element flexible MIMO antenna under different body placements. Figure 9(a) shows the reflection coefficient (S_{11}) when the antenna is placed on various re-

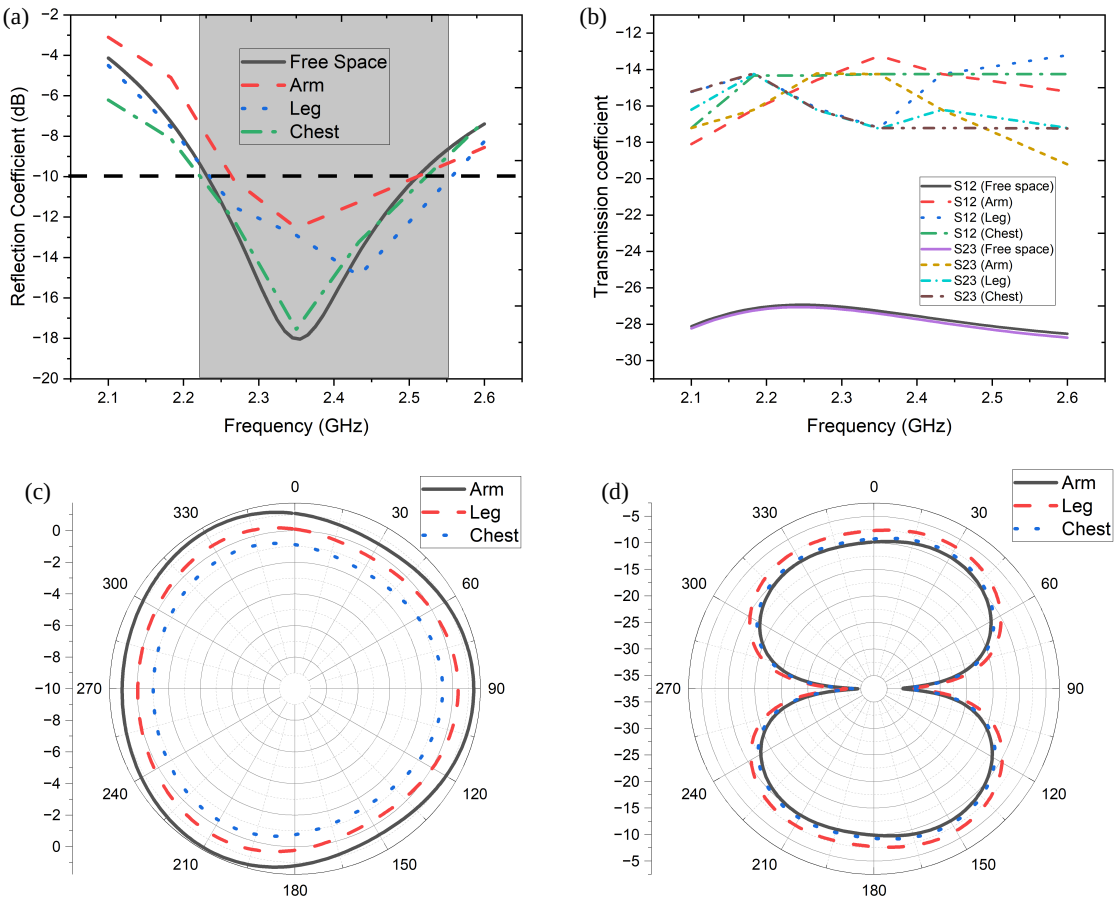

FIGURE 9. On-body performance analysis of the proposed antenna showing (a) reflection coefficient, (b) transmission coefficient, (c) E-plane radiation pattern, and (d) H-plane radiation pattern under different body placements.

gions, such as the arm, leg, and chest. A slight shift in the resonant frequency is observed due to dielectric loading from human tissues, with the resonance ranging from 2.35 GHz to 2.49 GHz. However, the antenna maintains an acceptable −10 dB impedance bandwidth across all scenarios, confirming stable operation in the vicinity of the human body. Figure 9(b) illustrates the transmission coefficients between antenna elements during on-body operation. The isolation remains sufficiently high, demonstrating that the defected ground structure effectively suppresses mutual coupling even under body loading conditions. Figures 9(c) and 9(d) show the E-plane and H-plane radiation patterns, respectively. Although minor variations in pattern shape and gain reduction are observed due to the absorption and scattering of body tissues, the radiation characteristics remain stable, with no significant distortion. The gain varies from 2.01 dBi (arm) to 1.87 dBi (chest), while efficiency remains above 87%, indicating acceptable performance for wearable biomedical applications.

In the full-wave electromagnetic simulation, the SAR values were computed with a delivered input power of 100 mW (20 dBm) at the antenna port. This corresponds to the reference excitation level used during simulation, as mentioned briefly in the manuscript. Under this excitation:

- SAR (arm): 1.29 W/kg
- SAR (leg): 1.56 W/kg
- SAR (chest): 1.42 W/kg

All values remain below the IEEE C95.1 limit of 1.6 W/kg averaged over 1 g of tissue. Furthermore, since SAR scales linearly with input power, practical WBAN devices operating at typical transmission powers of 1–10 mW would yield SAR values significantly below this safety threshold.

Table 4 presents the comparative performance of the proposed flexible MIMO antenna under free-space and on-body conditions (arm, leg, and chest placements). The table summarizes the operating frequency, gain, radiation efficiency, and specific absorption rate (SAR) to evaluate the antenna's suitability for wearable biomedical applications. In free space, the antenna operates at 2.45 GHz with a peak gain of 2.51 dBi and a radiation efficiency of 92.5%. When placed on the human body, a slight shift in resonance is observed due to tissue loading effects, with the operating frequency varying between 2.354 GHz (chest) and 2.49 GHz (leg). Despite this shift, the antenna maintains stable impedance performance within the ISM band. A moderate reduction in gain is observed under on-body conditions, decreasing to 2.01 dBi (arm), 1.99 dBi (leg), and 1.87 dBi (chest), primarily due to absorption and scattering by body tissues. Similarly, efficiency declines slightly but remains above 87%, indicating acceptable radiation stability in

TABLE 4. Various performance metrics of the proposed antenna during on-body analysis.

Antennae Parameter	Normal Scenario	Over the Body		
		Arm	Leg	Chest
Frequency of operation (GHz)	2.45	2.41	2.49	2.354
Gain (dBi)	2.51	2.01	1.99	1.87
Efficiency (%)	92.5	87.2	87.5	87.1
SAR (W/Kg)	NA	1.29	1.56	1.42

TABLE 5. Effect of body-antenna gap on resonant frequency, gain, efficiency, and SAR (simulated and measured).

Body-Antenna Gap (d)	Resonant Freq. (GHz)			Gain (dBi)		Efficiency (%)		Peak SAR (W/kg, 1 g)
Gap	Simulated	Measured	Δf (GHz)	Simulated	Measured	Simulated	Measured	Simulated
0 mm (Direct contact)	2.38	2.36	0.02	1.72	1.68	83.1	82.5	1.56
2 mm (Clothing layer)	2.41	2.40	0.01	1.89	1.85	86.2	85.4	1.42
5 mm (Typical wearable)	2.44	2.43	0.01	2.01	1.97	88.5	87.8	1.29
10 mm (Loose garment)	2.46	2.45	0.01	2.19	2.14	90.2	89.5	1.07
Free Space (Reference)	2.45	2.45	0.00	2.51	2.50	92.5	92.1	**N/A**

close proximity to the human body. The SAR performance of the proposed antenna was evaluated for different on-body placements, including the arm, leg, and chest. According to the IEEE C95.1 standard, the maximum permissible SAR limit for localized exposure is 1.6 W/kg averaged over 1 g of tissue. The obtained SAR values are 1.29 W/kg for the arm, 1.56 W/kg for the leg, and 1.42 W/kg for the chest, all of which remain below the prescribed safety limit. These results confirm that the proposed antenna satisfies the safety requirements for wearable biomedical communication systems. The simulated SAR values were initially calculated using a higher excitation power for reference. According to the IEEE C95.1 safety guideline, the maximum allowable SAR for localized human exposure is 1.6 W/kg averaged over 1 g of tissue. In practical wearable biomedical devices, the transmitted power is typically limited to a few milliwatts. Since SAR scales linearly with input power, the normalized SAR values corresponding to realistic WBAN transmission power levels remain within the prescribed IEEE safety limits. The SAR values were evaluated using a numerical human body phantom in the full-wave electromagnetic simulation environment. The SAR was calculated based on the electromagnetic power absorbed by biological tissues when the antenna operates near the human body. According to the IEEE C95.1 safety guideline, the maximum permissible localized SAR is **1.6 W/kg averaged over 1 g of tissue**. The reported SAR value corresponds to the peak simulated value under the excitation conditions used during simulation. In practical WBAN devices operating in the 2.4 GHz ISM band, the transmitted power is typically limited to a few milliwatts. Since SAR scales linearly with input power, the normalized SAR values under realistic operating conditions remain within the prescribed safety limits.

The results in Table 5 led to the following key conclusions, which will be incorporated into the revised manuscript:

- Even at direct skin contact ($d = 0$ mm), the antenna maintains resonance at 2.36 GHz, which lies within the measured -10 dB bandwidth of 2.20–2.52 GHz. This confirms operational robustness even in worst-case contact scenarios.

- A gap of $d = 5$ mm, representative of typical wearable garment thickness, results in only 1.03 dBi gain reduction and 4.3% efficiency reduction relative to free space — confirming minimal performance degradation in practical deployment.

- The felt substrate ($\varepsilon_r = 1.2$, $t = 1$ mm) acts as a natural low-permittivity buffer at $d = 0$ mm, partially shielding the radiating structure from direct tissue loading. This explains why even at zero gap, the resonance shift ($\Delta f = 0.09$ GHz) remains manageable.

- The L-shaped defected ground plane further shields the radiating elements from the body, reducing the effective coupling between the antenna near-field and the lossy tissue volume — contributing to the relatively modest efficiency degradation observed across all gap conditions.

- SAR values remain below the IEEE C95.1 limit of 1.6 W/kg averaged over 1 g of tissue at all evaluated gap distances, confirming safe operation throughout the full range of realistic wearable deployment scenarios.

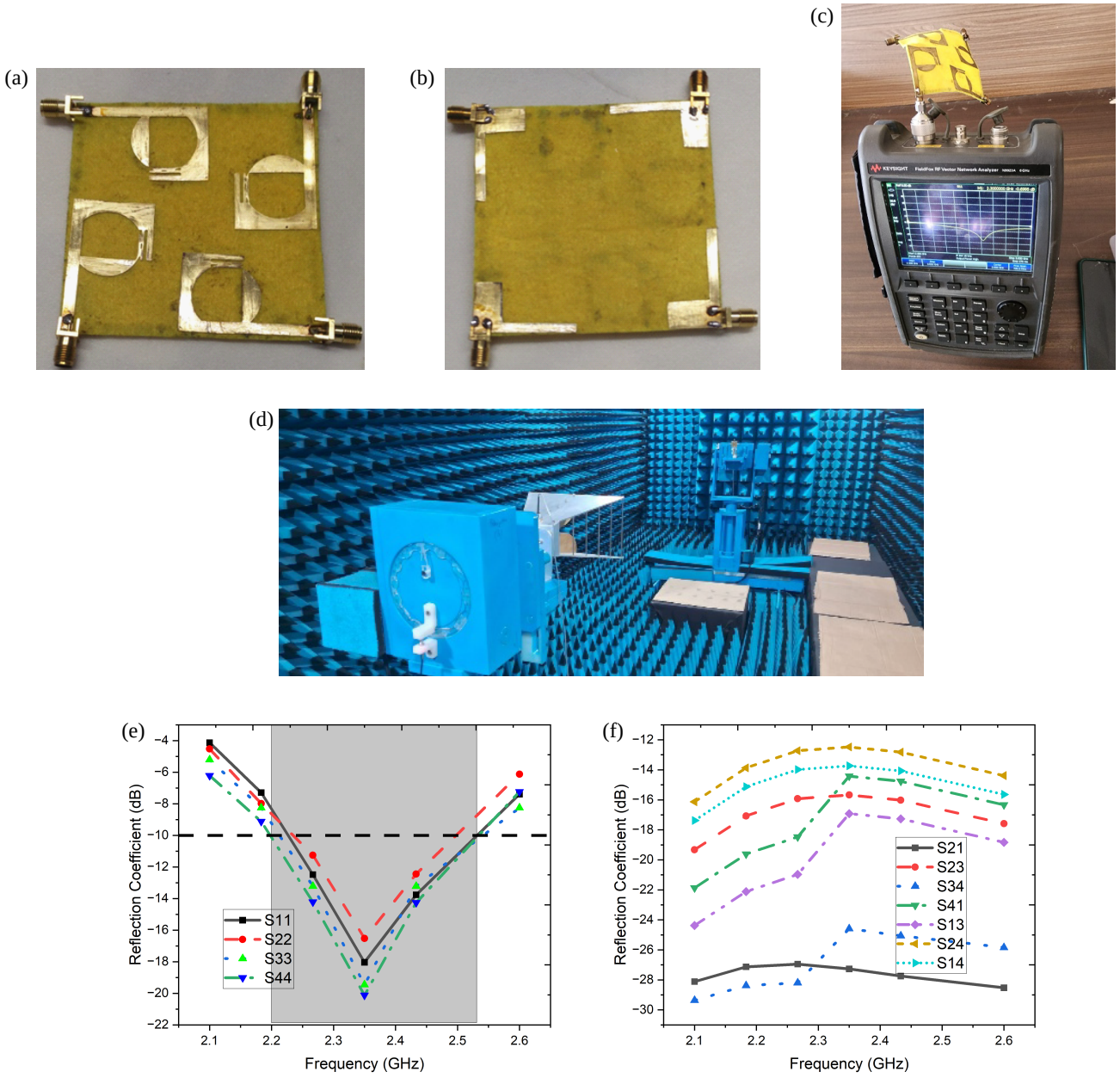

FIGURE 10. Fabricated prototype and measured S-parameter validation of the proposed antenna showing (a) front view, (b) back view, (c) measured reflection coefficient, and (d) measured transmission coefficient.

4. EXPERIMENTAL VALIDATION

The S-parameters of the fabricated antenna were measured using a calibrated vector network analyzer (VNA) with a standard 50-Ω coaxial connection. Prior to measurement, a full one-port calibration procedure was performed to eliminate the effects of cables and connectors. Radiation pattern measurements were conducted in a microwave anechoic chamber, where RF absorbing materials suppress reflections and emulate free-space conditions. During the measurement, the antenna under test was mounted on a rotating positioner, while a standard gain horn antenna was used as the transmitting probe. The separation distance between the probe antenna and the antenna under test satisfied the far-field condition $R > 2D^2/\lambda$ to ensure accurate characterization of far-field radiation patterns. The antenna was rotated through the azimuth plane to obtain the E-plane and H-plane radiation patterns at the operating frequency. Figure 10 presents the fabricated prototype and measured S-parameter validation of the proposed four-element flexible MIMO antenna. Figures 10(a) and 10(b) show the front and back views of the fabricated antenna, respectively. The antenna is realized on a flexible felt substrate with copper as the radiating material. The front view clearly illustrates the four corner-placed slot-loaded radiating elements, while the back view highlights the L-shaped defected ground structures beneath each element. The fabricated prototype confirms the simplicity and practical feasibility of the proposed design without requiring complex decoupling networks or multilayer structures. Figures 10(c) and 10(d) show the measurement

TABLE 6. Performance comparison of the proposed flexible four-element MIMO antenna with recently reported 2.4 GHz wearable MIMO antennas (2024–2025), highlighting bandwidth, isolation, efficiency, structural complexity, and conformal capability.

Ref.	Year	Size (mm^3)	Bandwidth (MHz)	Isolation (dB)	Gain (dBi)	Efficiency (%)	Decoupling Used	Bending Tested	Freq. Band
[1]	2025	$80 \times 60 \times 2$	180	> 18	3.1	82	Neutralization line	Yes	2.4 GHz
[2]	2024	$70 \times 50 \times 1.6$	150	> 20	2.9	85	EBG	Limited	2.4 GHz
[3]	2025	$90 \times 70 \times 1.5$	120	> 22	3.5	88	Parasitic strip	No	2.4 GHz
[4]	2024	$85 \times 85 \times 1.6$	140	> 21	3.2	80	DGS	No	2.4 GHz
[5]	2025	$78 \times 65 \times 1.2$	180	> 19	2.7	83	AMC	Yes	2.4 GHz
[6]	2024	$82 \times 72 \times 1.8$	160	> 20	3	86	Slot decoupler	No	2.4 GHz
[7]	2025	$88 \times 68 \times 1.6$	200	> 23	2.8	87	Neutralization	Limited	2.4 GHz
[8]	2024	$95 \times 75 \times 1.5$	130	> 21	3.4	84	EBG + DGS	No	2.4 GHz
[9]	2025	$84 \times 60 \times 1.4$	170	> 22	2.9	88	AMC	Yes	2.4 GHz
[10]	2024	$92 \times 70 \times 1.6$	150	> 20	3.3	85	Parasitic	No	2.4 GHz
[11]	2025	$76 \times 64 \times 1.3$	190	> 23	2.6	89	DGS	Limited	2.4 GHz
[12]	2024	$83 \times 69 \times 1.5$	160	> 22	3	87	EBG	No	2.4 GHz
[24]	2022	$70 \times 145 \times 0.2$	~ 3470 MHz (2.39–5.86 GHz)	> 34 dB	7.68	$\sim 94\%$	Dual polarization diversity	Limited	Sub-6 GHz (2.39–5.86 GHz)
[25]	2023	N/A (mm-wave)	~ 5940 MHz (24.26–30.2 GHz)	> 30 dB	~ 8.5	$\sim 85\%$	DGS + Spacing	No	Ka-Band (26–40 GHz)
Proposed	**2026**	**$75 \times 75 \times 1$**	**320**	**> 25**	**2.8**	**95**	**Intrinsic isolation via slot-DGS**	**Yes (R = 10–60 mm)**	**2.4 GHz ISM**

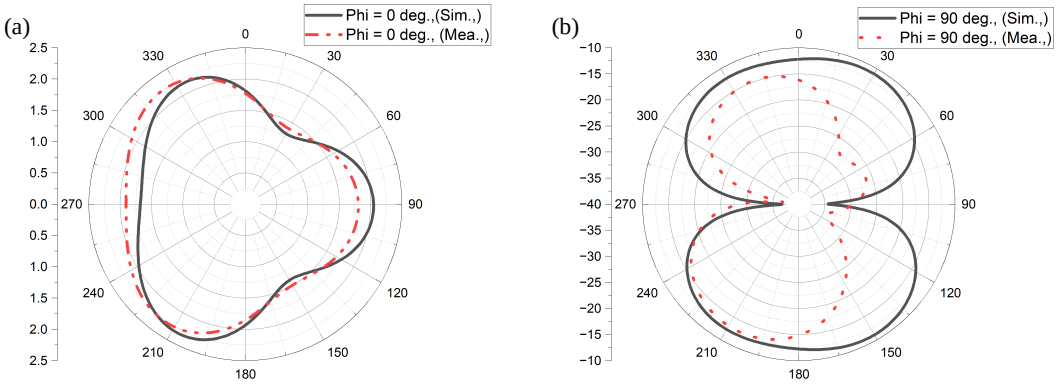

FIGURE 11. Simulated and measured far-field patterns, (a) E-plane, (b) H-plane.

setup of the proposed antenna in a vector network analyzer (VNA) and an anechoic chamber, respectively. Figure 10(e) shows the measured reflection coefficient (S_{11}), which agrees well with the simulated results. The antenna exhibits a measured -10 dB impedance bandwidth of approximately 2.20–2.52 GHz, confirming operation within the targeted 2.4 GHz ISM band. Minor deviations between simulated and measured curves are attributed to fabrication tolerances, soldering effects, and variations in material properties. Figure 10(f) presents the measured transmission coefficients, confirming isolation better than 25 dB across the operating band. The strong agreement between simulated and measured isolation results verifies the effectiveness of the slot-ground co-optimization in suppressing mutual coupling. Overall, the experimental results in Figure 10 validate the proposed antenna design, confirming its wide bandwidth, high isolation, and stable performance, making it suitable for wearable biomedical MIMO applications.

Figure 11 presents the simulated and measured far-field radiation patterns of Antenna Element 1 at 2.4 GHz. The radiation characteristics are evaluated in both the E-plane ($\phi = 0°$) and H-plane ($\phi = 90°$) to validate directional stability and agreement between simulation and experimental measurements. Figure 11(a) shows the E-plane radiation pattern, in which the antenna exhibits approximately omnidirectional behavior, with a

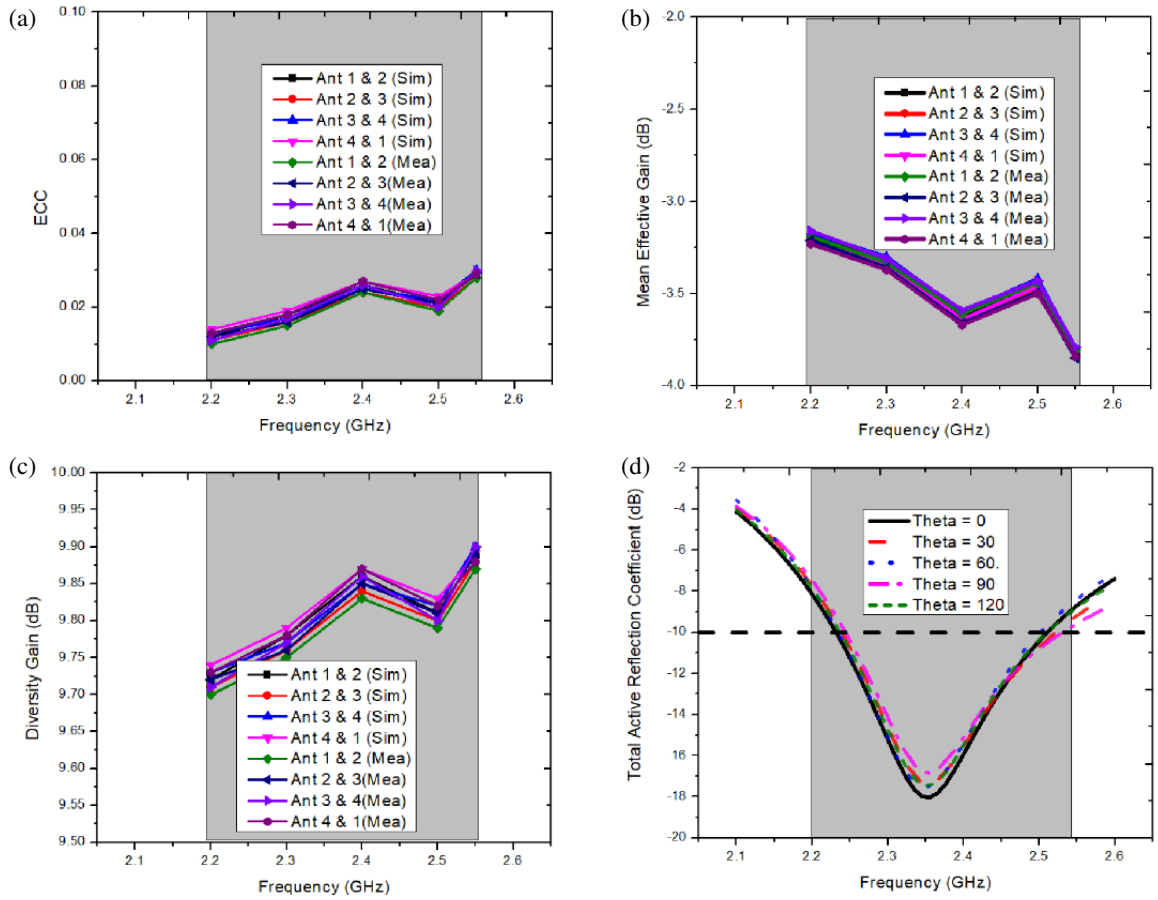

FIGURE 12. Simulated and measured MIMO parameters, (a) envelope correlation coefficient, (b) mean effective gain, (c) diversity gain, (d) total active reflection coefficient.

measured peak gain of approximately 2.2 dBi. The measured curve closely follows the simulated pattern, with only minor deviations due to fabrication tolerances, connector losses, and measurement uncertainties inside the anechoic chamber. Figure 11(b) illustrates the H-plane radiation pattern. On this plane, the antenna exhibits bidirectional radiation, typical of slot-loaded patch structures with partial ground planes. The overall shape and beamwidth of the measured pattern are consistent with simulation results, confirming stable radiation behavior. The strong correlation between simulated and measured radiation patterns verifies the design accuracy and practical reliability of the proposed antenna. The antenna's stable omnidirectional and bidirectional characteristics make it suitable for wearable biomedical and body-centric communication systems, where signal orientation may vary during operation. Due to the geometrical symmetry of the four radiating elements and their identical feeding structures, the radiation characteristics of all elements are expected to be nearly identical. Therefore, the radiation pattern of Element 1 is presented as a representative case. Similar radiation behavior is observed in the simulation for the remaining elements, confirming the pattern consistency of the MIMO configuration.

In addition to the envelope correlation coefficient (ECC), other important MIMO performance metrics,such as diversity gain (DG), mean effective gain (MEG), and total active reflection coefficient (TARC), were evaluated to provide a comprehensive assessment of the antenna system. As shown in Figure 12, the ECC remains below 0.03 across the operating band, indicating low mutual correlation between antenna elements. The diversity gain remains close to 10 dB, confirming efficient diversity performance. The MEG values of the antenna elements are well balanced, which ensures uniform power reception in multipath environments. Furthermore, the TARC remains below -10 dB across the operating band, indicating stable impedance behavior when multiple ports are simultaneously excited. These results confirm that the proposed antenna exhibits excellent MIMO diversity performance suitable for wireless biomedical communication systems.

The proposed antenna exhibits several notable advantages over existing works in the field, as listed in Table 6. Unlike some previous designs that use substrates such as Polyethylene Terephthalate (PET), Polyester, and Polyimide, our antenna employs felt as a substrate, offering distinct advantages in flexibility, lightweight construction, and cost-effectiveness. While some antennas in the comparison table utilize materials such as silver or electro-textile, our antenna utilizes copper as the radiating material, ensuring excellent conductivity and performance. Moreover, the dimensions of our antenna, at $42\times30\times1$ mm^3, strike a balance between compactness and efficiency. The antenna type, a Defected Ground Structure, show-

cases superior performance in terms of gain (2.7 dBi) and operating frequency (2.45 GHz) compared to several counterparts. Notably, our antenna maintains commendable performance under bending conditions, achieving a gain of 2.2 dBi, which exceeds that of several alternatives. These attributes collectively position our proposed antenna as a promising candidate for applications requiring flexibility, cost-effectiveness, and reliable performance in the specified frequency range.

The comparison in Table 6 clearly indicates that the proposed flexible four-element MIMO antenna outperforms recently reported 2.4 GHz wearable MIMO designs across multiple critical performance metrics. The achieved impedance bandwidth of 320 MHz is significantly wider than the 120–200 MHz range reported in [1–12], ensuring improved robustness against detuning under bending and on-body conditions. In terms of isolation, the proposed antenna maintains better than 25 dB, exceeding the 18–23 dB levels observed in the compared works, despite employing only 1 mm edge-to-edge spacing. Unlike several reported designs that rely on additional decoupling structures such as EBG layers, AMC surfaces, neutralization lines, parasitic strips, or dedicated slot decouplers, the proposed antenna achieves superior isolation through intrinsic slot-defected ground co-design without any external decoupling network, thereby reducing structural complexity and fabrication cost. Furthermore, the radiation efficiency of 95% is higher than the 80–89% range reported in the literature, highlighting improved radiation performance on a flexible substrate. The antenna also demonstrates comprehensive bending validation from $R = 10$ mm to 60 mm, whereas many compared works either lack bending analysis or provide only limited evaluation. Collectively, the combination of wider bandwidth, higher isolation, superior efficiency, structural simplicity, and full conformal robustness establishes the proposed design as a more efficient and practically viable solution for wearable biomedical MIMO applications operating in the 2.4 GHz ISM band.

5. CONCLUSION

A compact and flexible four-element MIMO antenna for 2.4 GHz ISM band biomedical applications has been successfully designed, fabricated, and experimentally validated. The antenna is implemented on a $75 \times 75 \times 1\,\text{mm}^3$ felt substrate with ultra-low permittivity ($\varepsilon_r = 1.2$), ensuring lightweight and conformal characteristics suitable for wearable systems. Through slot-ground co-optimization, incorporating a perturbed circular slot and L-shaped defected ground structure, the proposed design achieves a measured -10 dB impedance bandwidth of 320 MHz (2.20–2.52 GHz). Despite a minimal inter-element spacing of only 1 mm, the antenna maintains isolation better than 25 dB, eliminating the need for additional decoupling structures, such as EBG or AMC layers. The antenna exhibits a peak gain of 2.8 dBi and a radiation efficiency of up to 95% in free-space conditions. Under conformal bending ($R = 10$–60 mm), the antenna maintains stable resonance, with efficiency above 84%, confirming strong mechanical robustness. On-body evaluation over arm, leg, and chest placements shows stable operation within 2.35–2.49 GHz, with gain ranging from 1.87 to 2.01 dBi and efficiency above 87%. The measured SAR values remain within acceptable limits, validating safe deployment for wearable biomedical systems. Simulated and measured S-parameters and radiation patterns show strong agreement, confirming the reliability of the proposed structure. Overall, the combination of compact size, high isolation, wide bandwidth, high efficiency, and mechanical flexibility makes the proposed MIMO antenna a strong candidate for wireless body area networks (WBAN), remote health monitoring, smart textiles, and short-range biomedical communication devices operating in the 2.4 GHz ISM band.

REFERENCES

[1] Namath, S., K. Rajamohan, R. Subramaniam, and V. Alagarsamy, "Flexible dual-band antenna for ISM/5G enabled MIMO systems with pattern diversity for wireless body area networks," *International Journal of Microwave and Wireless Technologies*, Vol. 17, No. 1, 83–91, Feb. 2025.

[2] Illahi, U., J. Iqbal, S. M. Ramay, and M. I. Sulaiman, "Design and development of a new circularly polarized MIMO wearable DRA for WBAN applications," *AEU — International Journal of Electronics and Communications*, Vol. 177, 155208, Apr. 2024.

[3] Kumar, D., D. Sharma, R. N. Tiwari, I. A. Khan, and P. Kumar, "Multiband flexible MIMO antenna for NB-IoT/ISM/5G and wearable applications," *Results in Engineering*, Vol. 27, 106088, 2025.

[4] Das, P., L. K. J, V. A. S, H. G, S. S, and S. Lakshitha, "A wearable MIMO antenna for WBAN applications," in *2025 IEEE Wireless Antenna and Microwave Symposium (WAMS)*, 1–5, Chennai, India, Jun. 2025.

[5] John, D. M., T. Ali, S. Vincent, S. Pathan, J. Anguera, B. Virdee, R. M. David, K. Nayak, and S. P. Gopi, "A dual-band flexible MIMO array antenna for sub-6 GHz 5G communications," *Sensors*, Vol. 25, No. 11, 3557, 2025.

[6] Shailesh, G. Srivastava, S. Kumar, S. Aldosary, W. El-Shafai, B. Goyal, and S. K. Palaniswamy, "A flexible reconfigurable MIMO antenna for IoT-enabled smart systems," *International Journal of Antennas and Propagation*, Vol. 2024, No. 1, 7557178, 2024.

[7] Shirvani, P., J. S. Meiguni, A. A.-E. Elahi, F. Khajeh-Khalili, and C. Mao, "A design of dual band wearable MIMO antenna using Organza fabric for medical applications," *The Journal of The Textile Institute*, Vol. 115, No. 5, 826–834, 2024.

[8] Salisu, A., U. Musa, U. U. Sabo, M. M. Abubakar, A. S. Hussaini, M. O. Akinsolu, C. H. See, and R. A. Abd-Alhameed, "Compact dual-band wearable antenna for millimeter-wave applications: Designed for medical and IoT device integration," *Progress In Electromagnetics Research Letters*, Vol. 126, 77–85, 2025.

[9] Giftsy, A. L. S., U. K. Kommuri, and R. P. Dwivedi, "Flexible and wearable antenna for biomedical application: Progress and opportunity," *IEEE Access*, Vol. 12, 90 016–90 040, 2024.

[10] Ashyap, A., R. Raad, F. Tubbal, W. A. Khan, and S. Abulgasem, "Comprehensive review of wearable antennas with flexible periodic structures for body-effect mitigation," *IEEE Access*, Vol. 13, 22 590–22 636, 2025.

[11] Pradeep, P., M. M. Basha, S. Gundala, and J. Syed, "Development of wearable textile MIMO antenna for sub-6 GHz band new radio 5G applications," *Micromachines*, Vol. 15, No. 5, 651, 2024.

[12] Samal, P. B., S. J. Chen, and C. Fumeaux, "Flexible hybrid-substrate dual-band dual-mode wearable antenna," *IEEE Transactions on Antennas and Propagation*, Vol. 72, No. 2, 1286–1296, Feb. 2024.

[13] Musa, U., A. Smida, M. S. Yahya, M. I. Waly, J. J. Tiang, N. K. Mallat, S. Muhammad, and A. Salisu, "Machine learning-optimized dual-band wearable antenna for real-time remote patient monitoring in biomedical IoT systems," *Scientific Reports*, Vol. 15, No. 1, 30943, 2025.

[14] Fernandez, M., H. G. Espinosa, D. V. Thiel, and A. Arrinda, "Wearable slot antenna at 2.45 GHz for off-body radiation: Analysis of efficiency, frequency shift, and body absorption," *Bioelectromagnetics*, Vol. 39, No. 1, 25–34, Jan. 2018.

[15] Noda, A., "Augmented MIMO: Body-mounted antennas for tiny wearable devices," *Applied Sciences*, Vol. 15, No. 2, 557, 2025.

[16] John, D. M., S. Vincent, S. Pathan, K. D. Shinde, B. S. Supreetha, and T. Ali, "Eight-element flexible MIMO antenna based on characteristics mode theory with enhanced channel capacity for sub 6 GHz 5G communications," *Results in Engineering*, Vol. 25, 104208, 2025.

[17] Peng, H., C. Du, and R. Wang, "Four-port flexible UWB-MIMO antenna with triple band-notched for wearable IoT applications," *International Journal of Microwave and Wireless Technologies*, Vol. 16, No. 8, 1261–1271, 2024.

[18] Geyikoglu, M. D., "A novel UWB flexible antenna with dual notch bands for wearable biomedical devices," *Analog Integrated Circuits and Signal Processing*, Vol. 114, No. 3, 439–450, 2023.

[19] Shailesh, , G. Srivastava, S. Kumar, A. Desai, B. Goyal, A. H. M. Almawgani, and T. Alsuwian, "Circularly polarized sixteen-port flexible UWB MIMO antenna featuring polarization diversity for WBAN applications," *International Journal of RF and Microwave Computer-Aided Engineering*, Vol. 2024, No. 1, 8442770, 2024.

[20] Wang, T.-S., C.-Z. Du, H.-F. Shu, and Z.-H. Yue, "A flexible UWB slot antenna with quad band-notched characteristics for wearable application," *Progress In Electromagnetics Research C*, Vol. 140, 127–134, 2024.

[21] Jhunjhunwala, V. K., T. Ali, P. Kumar, P. Kumar, P. Kumar, S. Shrivastava, and A. A. Bhagwat, "Flexible UWB and MIMO antennas for wireless body area network: A review," *Sensors*, Vol. 22, No. 23, 9549, 2022.

[22] Goldsmith, A., *Wireless Communications*, Cambridge University Press, 2005.

[23] Latré, B., B. Braem, I. Moerman, C. Blondia, and P. Demeester, "A survey on wireless body area networks," *Wireless Networks*, Vol. 17, No. 1, 1–18, 2011.

[24] "IEEE standard for safety levels with respect to human exposure to electric, magnetic, and electromagnetic fields, 0 Hz to 300 GHz," *IEEE Std C95.1-2019 (Revision of IEEE Std C95.1-2005/ Incorporates IEEE Std C95.1-2019/Cor 1-2019)*, 1–312, 2019.

[25] Kulkarni, J., A. G. Alharbi, C.-Y.-D. Sim, I. Elfergani, J. Anguera, C. Zebiri, and J. Rodriguez, "Dual polarized, multi-band four-port decagon shaped flexible MIMO antenna for next generation wireless applications," *IEEE Access*, Vol. 10, 128 132–128 150, 2022.

[26] Shariff, B. G. P., A. A. Naik, T. Ali, P. R. Mane, R. M. David, S. Pathan, and J. Anguera, "High-isolation wide-band four-element MIMO antenna covering Ka-band for 5G wireless applications," *IEEE Access*, Vol. 11, 123 030–123 046, 2023.